Available online at www.sciencedirect.com
SCIENCE DIRECT®
Solid State Ionics 176 (2005) 731–743
SOLID STATE IONICS
www.elsevier.com/locate/ssi

H-bond network dynamics of the solid-state protonic conductor $Rb_3H(SeO_4)_2$ from FTIR and IINS measurements

G. Schuck[a,b,c,*], R.E. Lechner[b], K. Langer[c]

[a]ETH Zürich, Laboratory for Solid State Physics, CH-8093 Zürich, Switzerland
[b]Hahn-Meitner-Institut, Glienicker Strasse 100, D-14109 Berlin, Germany
[c]Institut für Angewandte Geowissenschaften, Technische Universität Berlin, Ernst-Reuter-Platz 1, D-10587 Berlin, Germany

Received 9 July 2004; accepted 3 November 2004

Abstract

Fourier transform infrared (FTIR) studies on small single crystals have been performed with the aim to analyse structural and dynamical aspects of the H-bond network in $Rb_3H(SeO_4)_2$. A comparative factor group analysis for both the monoclinic and the trigonal phase of $Rb_3H(SeO_4)_2$, based on centrosymmetric (C2/c and R$\bar{3}$m) and non-centrosymmetric (Cc, C2 and R3m) space group symmetries, has been carried out. Hypothetical structure models based on non-centrosymmetric space group symmetries are presented both for the monoclinic and the trigonal phase. They are shown to be of invaluable use in the interpretation of certain aspects of the observed vibrational spectra. In fact, our FTIR measurements and the comparative factor group analysis made clear that the centrosymmetric (time-averaged) structures are not sufficient for the description of the instantaneous and short-time/short-range order of the protons and for the related vibrational modes. Inelastic incoherent neutron scattering (IINS) spectra at 60, 100, 167 and 297 K are also reported. The OH bending mode (γOH) gives large IINS intensities. A detailed infrared (IR) band analysis between 800 and 1100 cm^{-1}, together with the IINS results, showed that the identified modes ($\nu_1[SeO_4]^{2-}$, $\nu_1[HSeO_4]^{1-}$, $\nu_3[SeO_4]^{2-}$ and $\nu_3[HSeO_4]^{1-}$) can be classified in two groups differing by the strength of the monomer coupling. Proton conductivity in $Rb_3H(SeO_4)_2$ crystals is shown to be due to a dynamic disorder in the form of an intracrystalline chemical equilibrium reaction: alternation between the association of the monomers $[HSeO_4]^{1-}$ and $[SeO_4]^{2-}$ resulting in the dimer $[H(SeO_4)_2]^{3-}$ (H-bond formation) and the dissociation of the latter into the two monomers (H-bond breaking).

Materials: $Rb_3H(SeO_4)_2$
Keywords: Comparative factor group analysis; Proton conduction; Intracrystalline chemical reaction

1. Introduction

The crystalline compound trirubidium hydrogen diselenate is a member of a family of proton conducting sulphates and selenates with the general formula $M_3H(XO_4)_2$ (M=K, Rb, Cs; X=S, Se). The high-temperature phase of $Rb_3H(SeO_4)_2$ with rhombohedral symmetry (trigonal R$\bar{3}$m space group) shows extremely high protonic conductivity of up to 3×10^{-2} Ω^{-1} cm^{-1} [1]; this phase is a solid-state protonic conductor (SSPC). The room temperature structure of $Rb_3H(SeO_4)_2$ (monoclinic A2/a space group; conventional setting C2/c) shows lower, but still appreciable protonic conductivities in a fairly broad temperature range in the vicinity of the SSPC phase transition [1,2]. The time-averaged crystal structure of $Rb_3H(SeO_4)_2$ can be described as a sequence of Rb-coordination polyhedra layers alternating with Rb...$H[SeO_4]_2$ layers [3,4]. Two selenate tetrahedra are connected by a hydrogen bond, forming an $H[SeO_4]_2^{3-}$ dimer. In the SSPC high-temperature phase (T>449 K), layers of two-dimensional dynamically disordered H-bond networks with trigonal symmetry are formed [4]. At low temperatures, these dimers form a so-called zero-dimensional hydrogen-bond network with centrosymmetric symmetry [3]. Note that the denomination "zero-

* Corresponding author. ETH Zürich, Laboratory for Solid State Physics, CH-8093 Zürich, Switzerland.
E-mail address: schuck@b-net.de (G. Schuck).

0167-2738/$ - see front matter © 2004 Elsevier B.V. All rights reserved.
doi:10.1016/j.ssi.2004.11.006

Table 1
The table contains the relative atomic coordinates (x, y, z) used for the monoclinic phase of $Rb_3H(SeO_4)_2$ (C2/c [3] and for the hypothetical structures C2 and Cc)

C2/c [3]				C2				Cc			
Atom	x	y	z	Atom	x	y	z	Atom	x	y	z
Rb(1)	0	0.2439	0.2500	Rb(1a)	0	0.2439	0.5000	Rb(1)	0	0.2439	0.2500
				Rb(1b)	0	0.7561	0				
Rb(2)	0.1945	0.2654	0.6519	Rb(2a)	0.1945	0.2654	0.9019	Rb(2a)	0.1945	0.2654	0.6519
				Rb(2b)	0.8055	0.7346	0.5981	Rb(2b)	0.8055	0.2654	0.8481
Se	0.1168	0.7731	0.4628	Se(a)	0.1168	0.7731	0.7128	Se(a)	0.1168	0.7731	0.4628
				Se(b)	0.8832	0.2269	0.7872	Se(b)	0.8832	0.7731	0.0372
O(1)	0.1572	0.9840	0.3995	O(1a)	0.1572	0.9840	0.6495	O(1a)	0.1572	0.9840	0.3995
				O(1b)	0.8428	0.0160	0.8505	O(1b)	0.8428	0.9840	0.1005
O(2)	0.0065	0.8233	0.4427	O(2a)	0.0065	0.8233	0.6927	O(2a)	0.0065	0.8233	0.4427
				O(2b)	0.9935	0.1767	0.8073	O(2b)	0.9935	0.8233	0.0573
O(3)	0.1547	0.7582	0.6213	O(3a)	0.1547	0.7582	0.8713	O(3a)	0.1547	0.7582	0.6213
				O(3b)	0.8453	0.2418	0.6287	O(3b)	0.8453	0.7582	0.8787
O(4)	0.1283	0.5430	0.3882	O(4a)	0.1283	0.5430	0.6382	O(4a)	0.1283	0.5430	0.3882
				O(4b)	0.8717	0.4570	0.8618	O(4b)	0.8717	0.5430	0.1118
H	0	0	0	H	0.0040	0.9770	0.2590	H	0.0040	0.9770	0.0090

Site occupation factors (SOF): C2/c—for all atoms SOF=1 (note that in Ref. [3] the H atom occupies x=0.004, y=0.9770 and z=0.0090 with SOF=1/2); C2 and Cc—for all atoms SOF=1. The Wyckoff letters (WL): C2/c—for all atoms WL=f(8), except for Rb(1), where WL=e(4) and H, where WL=a(2); C2—for Rb(1a) and Rb(1b), WL=b(2), otherwise 4(c) and Cc—for all atoms WL=4(a).

dimensional" points at the fact that neighbouring H-bonds are spatially isolated, i.e. they are not connected by H-bridges. With this common crystallographic model for the low temperature phase of $Rb_3H(SeO_4)_2$, the proton conductivity measured in this phase cannot be understood.

Recently evidence for breaking of the center of symmetry in zero-dimensional H-bonded $Rb_3H(SeO_4)_2$ has been reported, which leads to the non-centrosymmetric symmetry space group C2 for the low temperature phase and implies a new scheme in the solid state [5]. Polarized Raman scattering studies have shown the off-center positions of protons in the O–H…O bonds, which is equivalent to a non-centrosymmetric $H[SeO_4]_2^{3-}$ dimer [6].

Proton conductivity in $Rb_3H(SeO_4)_2$ is related to a dynamic disorder in the form of an intracrystalline chemical equilibrium reaction [7,8]. The diffusive proton motion relevant to the protonic conductivity is accessible to quasielastic incoherent neutron scattering (QINS) techniques [9–11]. In QINS studies on $Rb_3H(SeO_4)_2$ with a dynamic range from 1 μeV to 10 meV, the details of the mechanism of long-range proton diffusion were unravelled. A "trigonal asymmetric H-bond" (TAHB) model [12], based on the assumption of time-dependent potentials, agrees well with the measured QINS spectra [13,14].

Owing to its sensitivity to the vibrational displacements of the proton, inelastic incoherent neutron scattering (IINS) is another unique probe of the proton dynamics. This technique provides specific information complementary to that obtained from the Fourier transform infrared (FTIR) and Raman methods. Especially the OH bending modes, which give large IINS intensities, appear only weakly in the infrared spectra [30,31]. In the present work, special attention is given to IINS measurements at temperatures above 60 K.

The absorption spectra of $Rb_3H(SeO_4)_2$ in the infrared (IR) spectral region provide information on the symmetry of

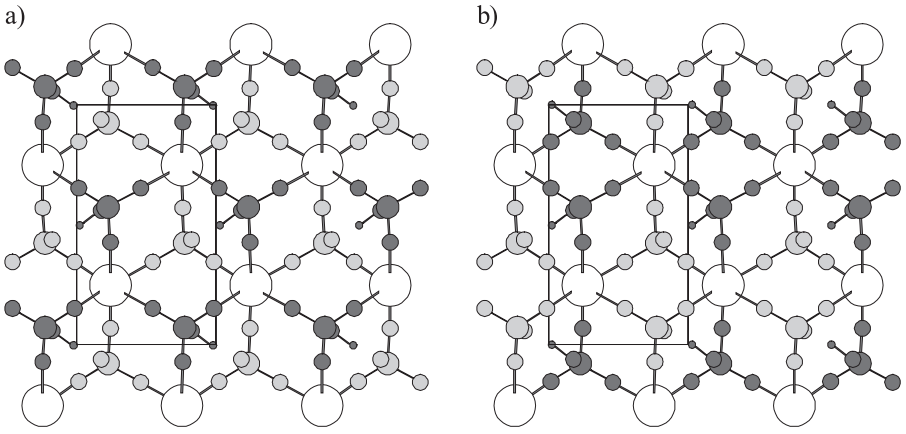

Fig. 1. The non-centrosymmetric hypothetical monoclinic structures of $Rb_3H(SeO_4)_2$; projection parallel (001); big white circles Rb(1); $[HSeO_4]^{1-}$ dark grey; $[SeO_4]^{2-}$ light grey; (a) Cc; (b) C2.

Table 2
Factor group analysis of $Rb_3H(SeO_4)_2$; monoclinic phase (Z^B: number of molecules per primitive Bravais cell, n_s: number of positions, t_γ : number of translations of a site species γ, C_ζ represents the degeneracy of the species ζ of the factor group, whereas a_ζ is the number of lattice vibrations of the equivalent set of atoms in species ζ of the factor group)

	Atoms	Site symmetry	n_s	γ	t_γ	f_γ	ζ	C_ζ	a_ζ	$\sum\Gamma_{Atom}$	$\Gamma_{acoustical}$
C2/c, Z=4, Z^B=2	$\Gamma_{transl.}$ Rb(1)	C_2 (2)	2	A (T_z)	1	2	A_g	1	1	A_g	
							A_u	1	1	A_u	
				B (T_x, T_y)	2	4	B_g	1	2	$2B_g$	
							B_u	1	2	$2B_u$	
	$\Gamma_{transl.}$ H	C_i ($\bar{1}$)	2	A_u (T_x, T_y, T_z)	3	6	A_u	1	3	$3A_u$	
							B_u	1	3	$3B_u$	
	$\Gamma_{transl.}$ Rb(2), Se, O(1), O(2), O(3), O(4)	C_1 (1)	4	A (T_x, T_y, T_z)	3	12	A_g	1	3	$18A_g$	
							A_u	1	3	$18A_u$	
							B_g	1	3	$18B_g$	
							B_u	1	3	$18B_u$	
	$\Gamma_{transl.}$ $Rb_3H(SeO_4)_2$	$\sum$ vibrational modes: $19A_g+22A_u+20B_g+23B_u$									A_u+2B_u
C2, Z=4, Z^B=2	$\Gamma_{transl.}$ Rb(1a), Rb(1b)	C_2 (2)	1	A (T_z)	1	1	A	1	1	2A	
				B (T_x, T_y)	2	2	B	1	2	4B	
	$\Gamma_{transl.}$ Rb(2a), Rb(2b), Se(a), Se(b), O(1a), O(1b), O(2a), O(2b), O(3a), O(3b), O(4a), O(4b), H(a)	C_1 (1)	2	A (T_x, T_y, T_z)	3	6	A	1	3	39A	
							B	1	3	39B	
	$\Gamma_{transl.}$ $Rb_3H(SeO_4)_2$	$\sum$ vibrational modes: 41A+43B									A+2B
Cc, Z=4, Z^B=2	$\Gamma_{transl.}$ Rb(1), Rb(2a), Rb(2b), Se(a), Se(b), O(1a), O(1b), O(2a), O(2b), O(3a), O(3b), O(4a), O(4b), H(a)	C_1 (1)	2	A (T_x, T_y, T_z)	3	6	A′	1	3	42A′	
							A″	1	3	42A″	
	$\Gamma_{transl.}$ $Rb_3H(SeO_4)_2$	$\sum$ vibrational modes: 42 A′+42A″									2A′+A″

the $H[SeO_4]_2^{3-}$ dimers. One goal of the elaborate factor group analysis is the possibility of a comparison between monoclinic and trigonal spectroscopic symmetries and the corresponding vibrational modes. This can be done by comparing these spectroscopic symmetries of the $H[SeO_4]_2^{3-}$ dimers in both phases. Here the dimers must be considered within their respective primitive Bravais cells (the monoclinic C2/c structure contains two and the trigonal $R\bar{3}m$ structure three primitive Bravais cells). In the present work, we report on results from FTIR spectra of small

Table 3
Internal vibrational modes of $Rb_3H(SeO_4)_2$; monoclinic phase; where v_i (i=1, 2,. . ., 4) are the vibrations of a tetrahedral ion with T_d symmetry (Herzberg notation)

C2/c	C2	Cc
Internal vibrational modes $[SeO_4]^{2-}$		
$\Gamma v_1=A_g+A_u+B_g+B_u$	Γv_1=A+B	Γv_1=A′+A″
$\Gamma v_2=2A_g+2A_u+2B_g+2B_u$	Γv_2=2A+2B	Γv_2=2A′+2A″
$\Gamma v_3=3A_g+3A_u+3B_g+3B_u$	Γv_3=3A+3B	Γv_3=3A′+3A″
$\Gamma v_4=3A_g+3A_u+3B_g+3B_u$	Γv_4=3A+3B	Γv_4=3A′+3A″
Lattice and libration vibrations $[SeO_4]^{2-}$		
$\Gamma_{libr.}=3A_g+3A_u+3B_g+3B_u$	$\Gamma_{libr.}$=3A+3B	$\Gamma_{libr.}$=3A′+3A″
$\Gamma_{transl.}=3A_g+3A_u+3B_g+3B_u$	$\Gamma_{transl.}$=3A+3B	$\Gamma_{transl.}$=3A′+3A″
Internal vibrational modes $[HSeO_4]^{1-}$		
$[SeO_4]^{2-}$ only	Γv_1=A+B	Γv_1=A′+A″
	Γv_2=2A+2B	Γv_2=2A′+2A″
	Γv_3=3A+3B	Γv_3=3A′+3A″
	Γv_4=3A+3B	Γv_4=3A′+3A″
	Γ_{OH}=3A+3B	Γ_{OH}=3A′+3A″
Lattice and libration vibrations $[HSeO_4]^{1-}$		
$[SeO_4]^{2-}$ only	$\Gamma_{libr.}$=3A+3B	$\Gamma_{libr.}$=3A′+3A″
	$\Gamma_{transl.}$=3A+3B	$\Gamma_{transl.}$=3A′+3A″
Lattice vibrational modes (cf. Table 2)		
$\Gamma_{Rb(1),\ Rb(2),\ H}=4A_g+7A_u+5B_g+8B_u$	$\Gamma_{Rb(1a),\ Rb(1b),\ Rb(2a),\ Rb(2b)}$=8A+10B	$\Gamma_{Rb(1a),\ Rb(1b),\ Rb(2a),\ Rb(2b)}$=9A′+9A″
$\sum$ *vibrational modes (optical+acoustical)*:		
$19A_g+22A_u+20B_g+23B_u$	41A+43B	42A′+42A″

Table 4
The table contains the relative atomic coordinates (x, y and z), the site occupation factor (SOF) and the Wyckoff letter (WL) with multiplicity (note that in Ref. [4] the O(2) atom occupies x=0.0445, y=−0.0445 and z=0.3370, with SOF=1/3)

$R\bar{3}m$ [4]						R3m					
Atom	x	y	z	SOF	WL	Atom	x	y	z	SOF	WL
Rb(1)	0	0	0	1	a(3)	Rb(1)	0	0	0	1	a(3)
Rb(2)	0	0	0.2030	1	c(6)	Rb(2a)	0	0	0.2030	1	a(3)
						Rb(2b)	0	0	0.7970	1	a(3)
Se	0	0	0.4104	1	c(6)	Se(a)	0	0	0.4104	1	a(3)
						Se(b)	0	0	0.5896	1	a(3)
O(1)	0.8119	0.1881	0.9013	1	h(18)	O(1a)	0.8119	0.1881	0.9013	1	b(9)
						O(1b)	0.1881	0.8119	0.0987	1	b(9)
O(2)	0	0	0.3370	1	c(6)	O(2a)	0	0	0.3370	1	a(3)
						O(2b)	0	0	0.6630	1	a(3)
H	0.5	0.5	0	1/3	e(9)	H	0	0	0.7107	1	a(3)

$Rb_3H(SeO_4)_2$ single crystals investigated in the temperature range between 298 and 503 K. We concentrated our analysis on the investigation of the ν_1 and ν_3 internal vibrational modes of $[SeO_4]^{1-}$ and $[HSeO_4]^{2-}$ groups [15] and the frequency region of the OH bending mode γOH which corresponds to a relatively small frequency range between 800 and 1100 cm^{-1}.

2. Comparative factor group analysis

In the literature already numerous results of factor group analysis on $Rb_3H(SeO_4)_2$ have been published, however, with conclusions not always consistent with each other [6,16,17]. In order to present a comparative factor group analysis for both the monoclinic and the trigonal phase of $Rb_3H(SeO_4)_2$, it is necessary to present this analysis in some more detail. In this context, an essential argument is the following: one may expect that the instantaneous and short-time (dynamic) structure will, in general locally and over short spatial ranges, not present the full symmetry of the time-averaged structures derived from conventional crystallographic studies. The latter may therefore not be sufficient to predict all the vibrational modes occurring in reality. It is consequently advisable to take into account the possible local short-time existence of structures with lower symmetries. For the monoclinic case, we consider C2/c [3] and two hypothetical non-centrosymmetric structures (Cc and C2 which are *translationengleiche* subgroups of C2/c) [14]. From the known C2/c site symmetries, the relative atomic positions and site symmetries in question for Cc and C2 were obtained (Table 1). As a result, we end up with two

Table 5
Factor group analysis of $Rb_3H(SeO_4)_2$; trigonal phase (Z^B: number of molecules per primitive Bravais cell, n_s: number of positions, t_γ : number of translations of a site species γ, C_ζ represents the degeneracy of the species ζ of the factor group, whereas a_ζ is the number of lattice vibrations of the equivalent set of atoms in species ζ of the factor group)

	Atoms	Site symmetry	n_s	γ	t_γ	f_γ	ζ	C_ζ	a_ζ	$\sum\Gamma_{Atom}$	$\Gamma_{acoustical}$
$R\bar{3}m$, Z=3, Z^B=1	Rb(1)	D_{3d} ($\bar{3}m$)	1	A_{2u} (T_z)	1	1	A_{2u}	1	1	A_{2u}	
				E_u (T_x, T_y)	2	2	E_u	2	1	E_u	
	Rb(2), Se, O(2)	C_{3v} (3m)	2	A_1 (T_x)	1	2	A_{1g}	1	1	$3A_{1g}$	
							A_{2u}	1	1	$3A_{2u}$	
				E (T_y, T_z)	2	4	E_g	2	1	$3E_g$	
							E_u	2	1	$3E_u$	
	O(1)	C_s (m)	6	A′ (T_x, T_y)	2	12	A_{1g}	1	2	$2A_{1g}$	
							A_{2u}	1	2	$2A_{2u}$	
							E_g	2	2	$2E_g$	
							E_u	2	2	$2E_u$	
				A″ (T_z)	1	6	A_{2g}	1	1	$1A_{2g}$	
							A_{1u}	1	1	$1A_{1u}$	
							E_g	2	1	$1E_g$	
							E_u	2	1	$1E_u$	
	$Rb_3H(SeO_4)_2$	$\sum$ vibrational modes: $A_{1u}+6A_{2u}+5A_{1g}+A_{2g}+7E_u+6E_g$									$A_{2u}+E_u$
R3m, Z=3, Z^B=1	Rb(1), Rb(2a), Rb(2b), Se(a), Se(b), O(2a), O(2b), H(a)	C_{3v} (3m)	1	A_1 (T_z)	1	1	A_1	1	1	$8A_1$	
				E (T_x, T_y)	2	2	E	2	1	8E	
	O(1a), O(1b)	C_s (m)	3	A′ (T_{xy})	2	6	A_1	1	2	$4A_1$	
							E	2	2	4E	
				A″ (T_z)	1	3	A_2	1	1	$2A_2$	
							E	2	1	2E	
	$Rb_3H(SeO_4)_2$	$\sum$ vibrational modes: $12A_1+2A_2+14E$									A_1+E

Table 6
Internal vibrational modes of $Rb_3H(SeO_4)_2$ with trigonal space group symmetries, where v_i (i=1, 2,…, 4) correspond to vibrations of the tetrahedral ion with T_d symmetry (Herzberg notation)

$R\bar{3}m$	R3m
Internal vibrational modes $[SeO_4]^{2-}$	
$\Gamma v_1=A_{1g}+A_{2u}$	$\Gamma v_1=A_1$
$\Gamma v_2=E_g+E_u$	$\Gamma v_2=E$
$\Gamma v_3=A_{1g}+A_{2u}+E_g+E_u$	$\Gamma v_3=A_1+E$
$\Gamma v_4=A_{1g}+A_{2u}+E_g+E_u$	$\Gamma v_4=A_1+E$
Lattice vibrations and libration vibrations $[SeO_4]^{2-}$	
$\Gamma_{libr.}=A_{2g}+A_{1u}+E_g+E_u$	$\Gamma_{libr.}=A_2+E$
$\Gamma_{transl.}=A_{1g}+A_{2u}+E_g+E_u$	$\Gamma_{transl.}=A_1+E$
Internal vibrational modes $[HSeO_4]^{1-}$	
$[SeO_4]^{2-}$ only	$\Gamma v_1=A_1$
	$\Gamma v_2=E$
	$\Gamma v_3=A_1+E$
	$\Gamma v_4=A_1+E$
	$\Gamma_{OH}=A_1+E$
Lattice and libration vibrations $[HSeO_4]^{1-}$	
$[SeO_4]^{2-}$ only	$\Gamma_{libr.}=A_2+E$
	$\Gamma_{transl.}=A_1+E$

Table 7
Distribution of internal vibrational modes $v_1[SeO_4]^{2-}$, $v_3[SeO_4]^{2-}$, $v_1[HSeO_4]^{1-}$ and $v_3[HSeO_4]^{1-}$; only infrared active modes are given; note that the trigonal modes are doubled in order to allow a comparison between the monoclinic and the trigonal phase

		Monoclinic			Trigonal	
		C2/c	Cc	C2	$R\bar{3}m$	R3m
$[SeO_4]^{2-}$	v_1	A_u+B_u	A′+A″	A+B	$2A_{2u}$	$2A_1$
	v_3	$3A_u+3B_u$	3A′+3A″	3A+3B	$2A_{2u}+2E_u$	$2A_1+2E$
$[HSeO_4]^{1-}$	v_1	$[SeO_4]^{2-}$ only	A′+A″	A+B	$[SeO_4]^{2-}$ only	$2A_1$
	v_3		3A′+3A″	3A+3B		$2A_1+2E$

possible arrangements for the $[HSeO_4]^{1-}$ and $[SeO_4]^{2-}$ groups in these hypothetical monoclinic $Rb_3H(SeO_4)_2$ structures (Fig. 1).

The factor groups are 2/m for C2/c, m for Cc and 2 for C2. In all three cases, the crystallographic unit cell contains two primitive Bravais cells. Via the correlation procedure [18] we identified the species γ of the translation T_i for each site symmetry and ended up with the same number of 81 optical vibration modes ($3N-3$) in each case, but with different spectroscopic symmetry types (Table 2), 42 infrared active lattice vibrations (A_u, B_u) for C2/c, but 81 infrared active lattice vibrations in the case of C2 (A, B) and Cc (A′, A″).

$Rb_3H(SeO_4)_2$ crystals not only possess lattice vibrations but also libration and intramolecular vibrations of the $H[SeO_4]_2^{3-}$ dimers. The correlation technique [18] is used to predict number and type of intramolecular vibrations (Table 3). The $[SeO_4]^{2-}$ ions occupy sites of site symmetry C_1 (1) in the case of C2/c. We calculate the lattice vibrations ($\Gamma_{transl.}$) and the librations ($\Gamma_{libr.}$) of the $[SeO_4]^{2-}$ group and must add 24 lattice vibrational modes for Rb(1), Rb(2) and H, so that again we end up with 81 optical modes. For C2 and Cc, the $H[SeO_4]_2^{3-}$ dimer can be separated into $[HSeO_4]^{1-}$ and $[SeO_4]^{2-}$ monomers, each with C_1 (1) site symmetry. Using the correlation technique, we obtain the lattice and the librational modes and the internal vibrational modes of the $[HSeO_4]^{1-}$ and $[SeO_4]^{2-}$ groups. If we take into account the 18 lattice modes, this leads to 81 optical modes.

In the trigonal case, we consider $R\bar{3}m$ [4] and a hypothetical structure with space group symmetry R3m (*translationengleiche* subgroup of $R\bar{3}m$). The additional site symmetries and relative atomic positions for R3m are summarized in Table 4. In our hypothetical trigonal structure model, the hydrogen atom is situated on top of the $[SeO_4]^{2-}$ group forming a hydrogen bond (O(2b)–H) with a distance of 1.08 Å, which builds an $[HSeO_4]^{1-}$ group. The factor groups are $\bar{3}m$ for $R\bar{3}m$ and 3m for R3m. The number of molecules per primitive Bravais cell Z^B is one in both cases (Table 5). The number N of atoms per primitive Bravais cell is 14, so that we expect 39 optical modes ($3N-3$).

In order to accomplish the factor group analysis for $R\bar{3}m$, we must consider the disorder of the O(2) atom and the H atoms. We must keep in mind the limited validity of selection rules in the presence of disorder in crystals [16]. So we can use only complete atoms and not "splitted" ones to find a realistic picture of the vibrational motions in

Table 8
Results of spectra fits of temperature-dependent IINS measurements of $Rb_3H(SeO_4)_2$ with TFXA; for comparison literature data are given [30]

Temperature	This paper				Literature data [30]			Assignment
	60 K	100 K	167 K	297 K	5 K	40 K	60 K	
Wave number (cm^{-1})	35.5	37.4	39.0	37.8	–	–	–	
	104.1	102.2	99.9	95.8	–	–	–	
	131.1	129.4	126.5	117.7	–	–	–	
	219.5	211.1	197.6	171.2	–	–	–	
	292.6	296.0	296.6	–	–	–	–	
	–	–	–	–	328.3	332.3	–	
	335.2	336.8	334.2	331.3	341.2	346.0	337.2	$v_2[SeO_4]^{2-}$
	407.7	408.5	404.3	401.2	408.9	410.6	408.9	$v_4[SeO_4]^{2-}$
	1092.5	1087.9	1075.4	1045.9	1097.0	1098.6	1096.2	γOH
	1526.8	1519.1	1506.1	1467.4	1535.0	1536.6	1533.3	δOH

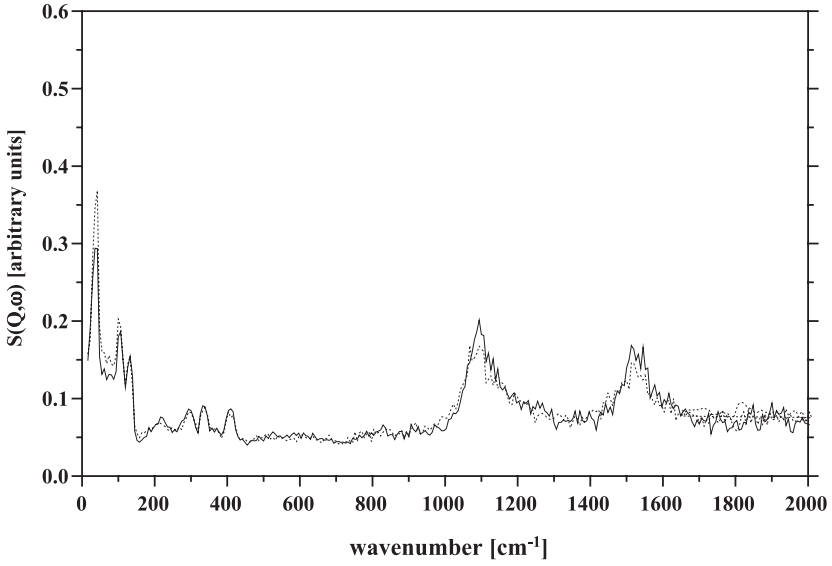

Fig. 2. IINS spectra of $Rb_3H(SeO_4)_2$ at 60 K (solid line) and 100 K (dotted line). The spectra were measured with the TFXA spectrometer at Rutherford Appleton Laboratory.

$Rb_3H(SeO_4)_2$ crystals (there are only $3N-3$ degrees of freedom for the optical motion in crystals). As example we regard the hydrogen atom, this atom is disordered over the three-fold 9(e) sites (x=0.5, y=0.5, z=0; SOF=1/3; model "A" in Ref. [4]). If we carry out the factor group computation for this disordered hydrogen atom, we find nine vibrational modes ($A_{1u}+E_u+2A_{2u}+2E_u$) and not three modes, as it should be [6,16]. It is not possible to divide the result in a useful way or to find a non-disordered position for the hydrogen in the centrosymmetric trigonal structure, and therefore this atom cannot be included into this comparative factor group analysis. Without hydrogen, we expect only 36 optical modes ($3\times13-3$). The O(2) atoms are disordered over the three-fold h(18) sites. In order to carry out the factor group analysis for O(2), we assumed for these atoms the position 0,0,z (c(6) site). For $R\bar{3}m$, we obtain 17 lattice vibrations ($5A_{2u}$, $6E_u$) that are only infrared active and 15 vibrations that are only Raman active ($5A_{1g}$, $5E_g$), whereas for the non-centrosymmetric space group symmetry (R3m), 37 vibrations that are both infrared and Raman active ($11A_1$, 13E) can be found (Table 5).

We finish the comparative factor group analysis for the trigonal phase with the prediction of the intramolecular vibrations. The $[SeO_4]^{2-}$ ions in the $R\bar{3}m$ case occupy a site of site symmetry C_{3v} (3m). For R3m, the $H[SeO_4]_2^{3-}$ dimer can be separated into $[HSeO_4]^{1-}$ and $[SeO_4]^{2-}$ monomers each with C_{3v} (3m) site symmetry (Table 6).

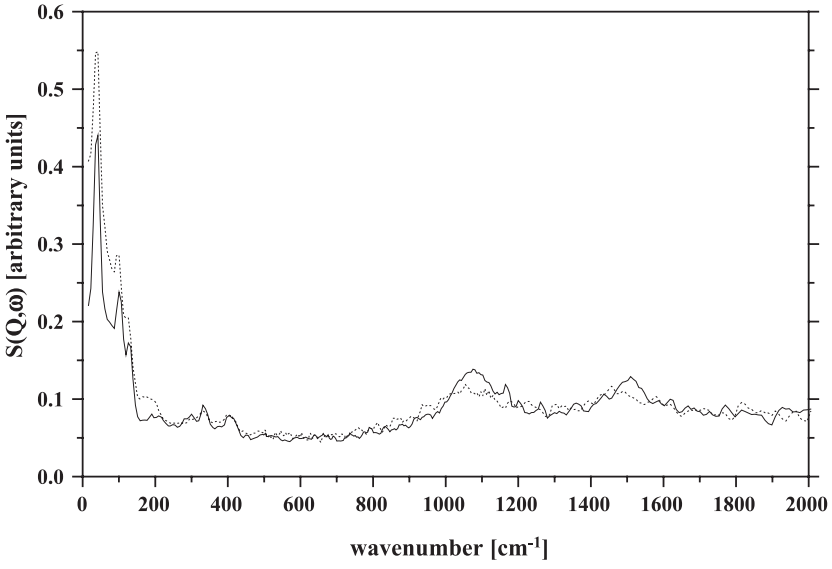

Fig. 3. IINS spectra of $Rb_3H(SeO_4)_2$ at 167 K (solid line) and 297 K (dotted line). The spectra were measured with the TFXA spectrometer at Rutherford Appleton Laboratory.

As a result of the factor group analysis, we are now able to compare the internal vibrational modes $\nu_1[SeO_4]^{2-}$, $\nu_3[SeO_4]^{2-}$, $\nu_1[HSeO_4]^{1-}$ and $\nu_3[HSeO_4]^{1-}$ in the monoclinic and the trigonal phase of $Rb_3H(SeO_4)_2$ (Table 7).

3. Analysis of IINS spectra

Inelastic incoherent neutron scattering (IINS) spectra were obtained with the spectrometers Neutron Energy Analysis by Time-of-Flight (NEAT) [27,28] and Time Focused Crystal Analyser (TFXA) [29]. Only the latter will be discussed here. The $Rb_3H(SeO_4)_2$ powder sample was enclosed in a vanadium cylinder with 60 mm height, 5 mm thickness and 30 mm width. The measurements were carried out at four different temperatures; 60, 100, 167 and 297 K. For the operation of the TFXA spectrometer, neutrons of the ISIS pulsed neutron source at the Rutherford Appleton Laboratory (Chilton, UK) were used. At every ISIS pulse, a white spectrum of incident neutrons illuminated the powder sample, at 12.13 m from the source. Some of those neutrons, with sufficient energy to cause an internal excitation or deexcitation in the sample, were scattered towards the secondary spectrometer that viewed the sample at a scattering angle of 135° and used a pyrolytic graphite (002) crystal to select the final neutron energy of 3 meV (24 cm^{-1}). These neutrons were diffracted onto the detector assembly, passing through a beryllium filter on the way to eliminate the higher order Bragg reflections. A monitor spectrum was also collected for each measurement for the

Table 9
Observed frequencies within the frequency range of internal vibrational modes $\nu_1[SeO_4]^{2-}$ and $\nu_3[SeO_4]^{2-}$ in $Rb_3H(SeO_4)_2$, H_2SeO_4 and $KHSeO_4$ at several temperatures (RT: room temperature; IR: infrared measurements; RA: Raman scattering measurements)

Wave number (cm^{-1})	$Rb_3H(SeO_4)_2$						H_2SeO_4	$KHSeO_4$		$Rb_3H(SeO_4)_2$		
	This paper	[19]	[17]	[20]	[6]	[21]	[22]	[23]		This paper	[6]	[21]
	298 K	RT	RT	RT	300 K	301 K (79 K)	RT	RT	RT	503 K	450 K	483 K
	IR	IR	IR	RA	RA	RA	RA	IR	RA	IR	RA	RA
800											800	
805												
810	810*[1]									812*[1]		
815									817			
820												
825											828*[5]	826*[5]
830								830		833*[2]		
835	837*[2]						837					
840												
845			845ν_1						847			
850												
855												
860							862			863*[6]		864ν_1
865				866ν_1		866ν_1					867ν_1	
870	874*[6]				870ν_1	(873)ν_1						
875							875			878*[7]		
880	882*[7]											
885								888				
890				890ν_3						894*[3]	894ν_3	
895				899ν_3	898ν_3		898					896ν_3
900	903*[3]	904ν_3	902ν_3	904ν_3		(900)ν_3					900ν_3	
905					907ν_3	904ν_3			908	908*[4]		
910						(908)ν_3		913				
915	918*[4]					(915)ν_3	915					
920										923*[8]		
925											925ν_3	
930	933*[8]											
935									937	939*[8]		
940												
945	948*[8]						945					
950												
955								958	957			
960												
965												
970												
975							975					

Band assignment: strongly coupled $H[SeO_4]_2$ dimer: *[1]: $\nu_1[SeO_4]^{2-}$; *[2]: $\nu_1[HSeO_4]^{1-}$; *[3]: $\nu_3[SeO_4]^{2-}$; *[4]: $\nu_3[HSeO_4]^{1-}$. Band assignment: weekly coupled $H[SeO_4]_2$ dimer: *[5]: $\nu_1[SeO_4]^{2-}$ (only Raman active); *[6]: $\nu_1[HSeO_4]^{1-}$; *[7]: $\nu_3[SeO_4]^{2-}$; *[8]: $\nu_3[HSeO_4]^{1-}$.

normalization of the data. The measured data sets were converted from time of flight spectra into energy spectra with the program REHACK [29].

The energy spectra are shown in Figs. 2 and 3. Frequencies and band assignments are summarized in Table 8. At 60 K, between 200 and 500 cm^{-1}, four bands could be observed. These bands become broader with increasing temperature. The two bands between 330 and 410 cm^{-1} could be assigned as ν_2 and ν_4 vibrational modes of the selenate group. No IINS bands are observed in the frequency range of the symmetric and anti-symmetric vibrational modes of selenate (ν_1 and ν_3), between 800 and 950 cm^{-1}. Two very broad OH modes, γOH and δOH, are observed between 1000 and 1600 cm^{-1}. The measured intensities of the γOH and δOH modes are similar for each temperature in the whole temperature range. The frequency of the OH bending mode (γOH) decreases from 1092.5 cm^{-1} at 60 K to 1045.9 cm^{-1} at room temperature (297 K). The δOH mode also exhibits a similar behavior of the frequency. The intensity of the IINS bands at higher wave numbers (between 1000 and 1600 cm^{-1}), especially at higher temperatures, is lower due to the strong influence of the Debye-Waller factor. The influence of phonon wings [31] at higher wave numbers becomes stronger at increasing temperatures. In contrast to the intensity decrease in the region of higher wave numbers at higher temperatures, an intensity increase is observable at lower wave numbers, especially between 30 and 120 cm^{-1}.

4. Analysis of FTIR spectra and band assignment

The measurements to be discussed here were taken with a Bruker IFS66/MCT-D26 FTIR-microscope spectrometer on small (30×30×3 μm) pseudohexagonal $Rb_3H(SeO_4)_2$ single crystals that are grown on a gold lattice (TEM-gold lattice, 600 Mesh) by recrystallization [14]. Only single domain crystals are used. The optical behavior of the measured crystals was tested using a polarizing microscope. Measurements on larger $Rb_3H(SeO_4)_2$ crystals are not possible because of strong absorption bands (Fig. 4b and c). The accuracy of the frequencies was ±0.5 cm^{-1} and the accuracy of the temperature was about ±0.1 K. Temperature dependent (298–503 K) unpolarized transmission spectra on $Rb_3H(SeO_4)_2$ small crystals were measured between 4000 and 400 cm^{-1} (Fig. 4a). Partial drastic intensity changes could be observed. The temperature dependences of the infrared spectra within the frequency range of internal vibrational selenate modes ν_1 and ν_3 (800 to 1100 cm^{-1}) in $Rb_3H(SeO_4)_2$ are shown in Fig. 5.

Close examination of the spectrum of small $Rb_3H(SeO_4)_2$ crystals in the frequency range from 800 to 1100 cm^{-1} reveals nine IR bands of varying intensity. In order to limit the number of fitting parameters and thus to find a reasonable model, we restricted our fit model to the relatively small frequency range from 800 to 1100 cm^{-1}. We were able to find a good fitting model for the measured spectra for both the monoclinic (Fig. 6) and the trigonal phase (Fig. 7). This model consists of nine Gaussian functions as well as three background functions. The background functions are necessary to model the surrounding frequency ranges. The latter include underlying bands that are very broad (HWHM of about 100 cm^{-1}) as compared to the bandwidths of the lines studied in our work in the considered frequency range from 800 to 1100 cm^{-1}. The latter lines have widths one order of magnitude smaller [14]. The broad background bands, which are centered outside of this range, are partially overlapping with it (see Fig. 4). The behavior of the full width at half maximum shows only a weak temperature dependence, so

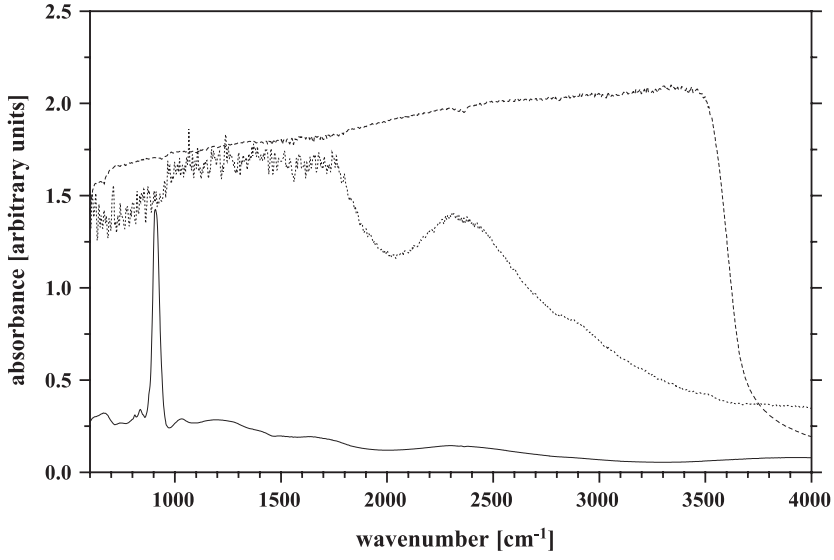

Fig. 4. Infrared single crystal spectra of (a) a small $Rb_3H(SeO_4)_2$ crystal (30×30×3 μm) at 298 K (solid line) and of large $Rb_3H(SeO_4)_2$ crystals demonstrate that the latter are showing strong absorption bands: (b) 50-μm-thick crystal (dashed line) and (c) 20-μm-thick crystal (dotted line).

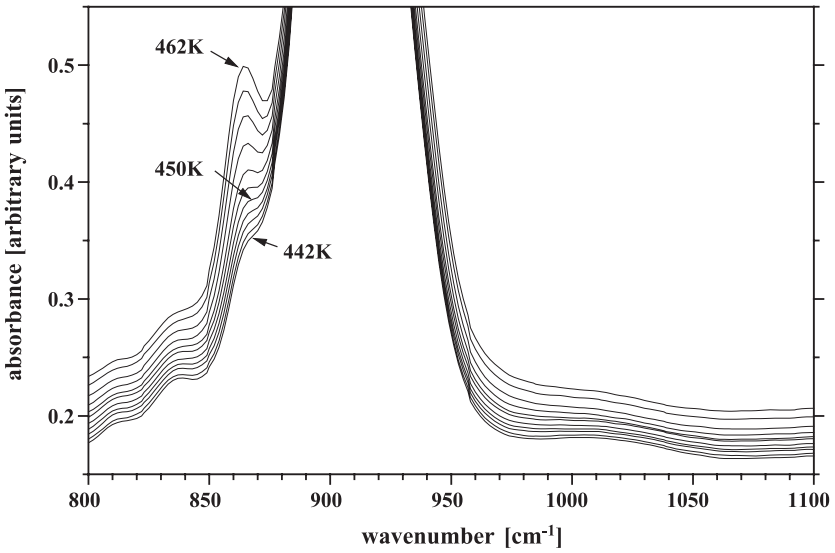

Fig. 5. T-dependence across the SSPC phase transition (T_c=449 K); infrared single crystal spectra of a small $Rb_3H(SeO_4)_2$ crystal (30×30×3 μm); temperature range: 442 to 462 K; temperature-steps of ΔT=2 K; the spectral band at 873.5 cm^{-1} (frequency at 298 K) shows a drastic change of intensity in the neighbourhood of the phase transition.

that constant widths for all temperatures (HWHM=8 cm^{-1} in the case of the bands 810.4, 837.3, 873.5 and 881.8 cm^{-1}; HWHM=29.7 cm^{-1} for the band 1027.2 cm^{-1}; frequency values at 298 K), and an HWHM with linear temperature dependence in the case of the bands 902.5, 918.0, 933.0 and 947.6 cm^{-1} (HWHM [cm^{-1}]=8.3 [cm^{-1}]+ 0.035 [cm^{-1} °C^{-1}]×T [°C]; frequency values at 298 K), respectively, could be used in our fit model.

The frequencies generally show somewhat larger temperature dependences than the half widths. All frequencies become smaller with increasing temperature. Linear functions for the description of the monotonous temperature behavior are used for the two bands 810.4 and 837.3 cm^{-1}. The bands at 902.5 and 918.0 cm^{-1} exhibit a discontinuous behavior of the frequency near the phase transition (Fig. 8). Almost all vibrational modes in the frequency range between 800 and 1100 cm^{-1} exhibit strong temperature dependences of their amplitudes (Fig. 9). The modes can be divided into two groups. In a first group, the intensities increase with increasing temperature (933.0, 947.6 and 873.5 cm^{-1}; frequency values at 298 K); here the largest effect is observed on the 873.5 cm^{-1} band (the amplitude at 505 K is more than 12 times larger than that at 298 K). In the second group, the vibrational modes exhibit an inverse intensity behavior; here the intensities decrease

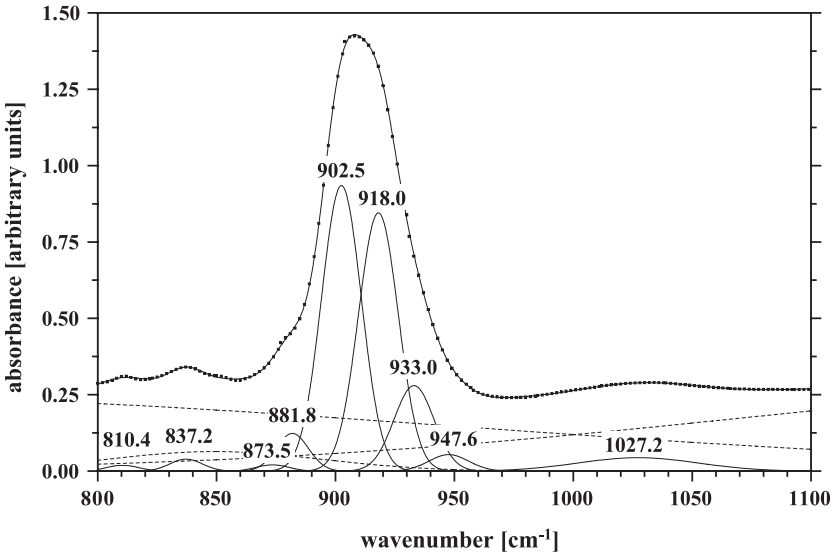

Fig. 6. Infrared spectra of $Rb_3H(SeO_4)_2$ between 800 cm^{-1} and 1100 cm^{-1} at 298 K (monoclinic phase); measurements of a small crystal (30×30×3 μm) using the Bruker IFS66/MCT-D26 FTIR-microscope spectrometer; fit of the measured spectra with nine Gaussian functions, as well as with three background functions (dashed).

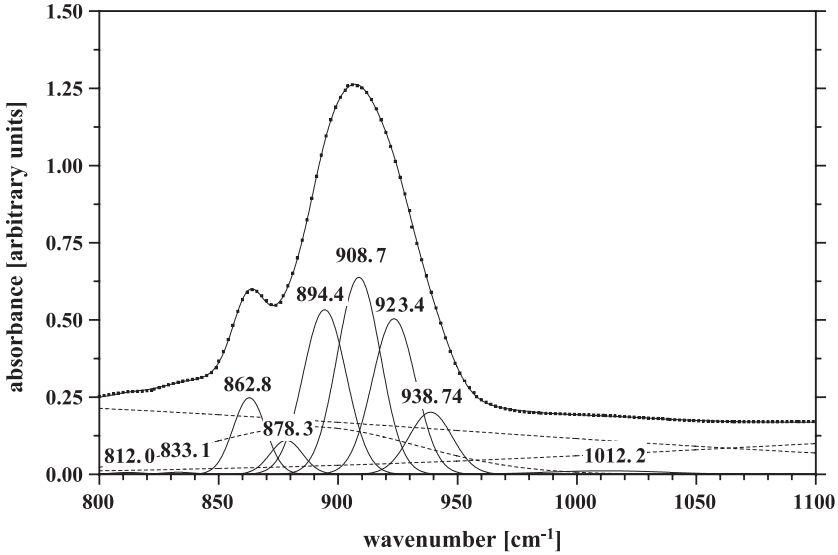

Fig. 7. Infrared spectra of $Rb_3H(SeO_4)_2$ between 800 and 1100 cm^{-1} at 503 K (trigonal phase); measurements of a small crystal (30×30×3 μm) using the Bruker IFS66/MCT-D26 FTIR-microscope spectrometer; fit of the measured spectra with nine Gaussian functions as well as with three background functions (dashed).

with increasing temperature (810.4, 837.3, 902.5, 918.0 and 1027.2 cm^{-1}; frequency values at 298 K), whereby the strongest effect is observed at 837.3 cm^{-1}.

The nine bands observed in the IR spectra, characteristic of internal vibrational modes in $Rb_3H(SeO_4)_2$, were assigned by comparison with literature data ($Rb_3H(SeO_4)_2$ [6,17,19–21], H_2SeO_4 [22] and $KHSeO_4$ [23]), together with the results of the comparative factor group analysis and with the IINS results [14]. In the range of strong OH bondings (O. . .O distance from 2.4 up to 2.6 Å), the band at 1027.2 cm^{-1} (at 298 K) might be assigned either as OH stretching mode (νOH) or as OH bending mode (γOH), at first sight. Through a comparison of spectroscopic (FTIR and IINS) results and crystallographic literature data (frequency as a function of O(2)–O(2)′ distance) an assignment as OH bending mode (γOH) seems however warrantable (Figs. 10 and 11).

The selenate band assignment is not possible with the assumption of centrosymmetric space group symmetries. This is due to the fact that for these symmetries we would expect a decrease of the number of observable bands through degeneration at higher temperatures. In the centrosymmetric monoclinic case, we expect eight and in the centrosymmetric trigonal case we expect six infrared active modes (Table 7); but the degeneration is in fact not observed. We clearly observe more than six bands at higher temperatures (Table 9). Phenomenologically, it seems that the IR spectra of $Rb_3H(SeO_4)_2$ have substantial similarity with IR spectra of selenium acid [22], $KHSeO_4$ [23] or other compounds in which $[HSeO_4]^{1-}$ and $[SeO_4]^{2-}$ modes are

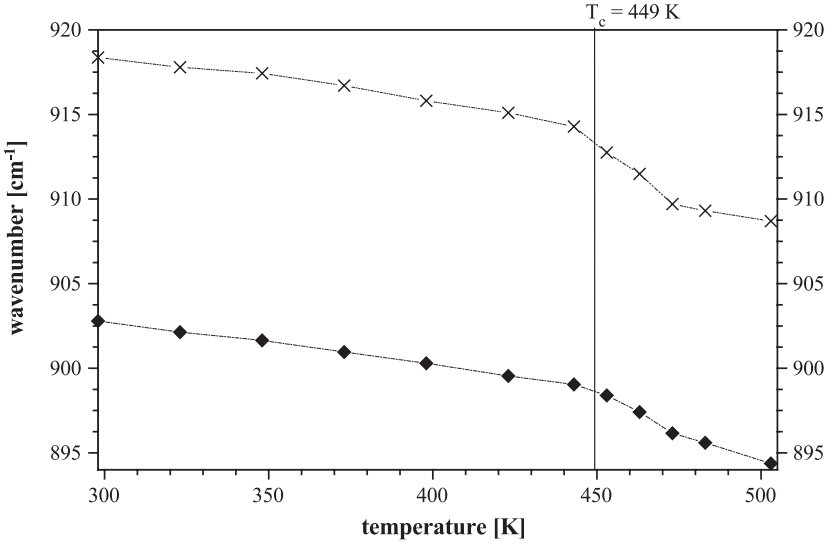

Fig. 8. Temperature dependence of frequencies of the two bands 902.5 and 918.0 cm^{-1} (frequencies at 298 K).

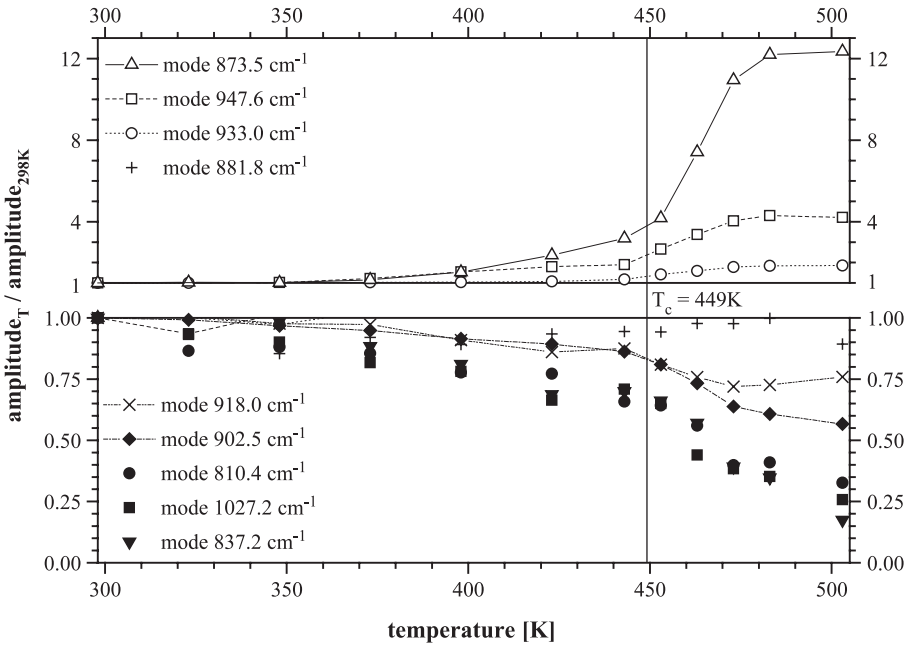

Fig. 9. The vibrational modes between 800 and 1100 cm^{-1} exhibit strong temperature dependences of their amplitudes; frequencies in legend at 298 K.

observed both at the same time. Together with the reported evidence for non-centrosymmetric symmetry [5], it therefore appears justifiable to assign $[HSeO_4]^{1-}$ modes and $[SeO_4]^{2-}$ modes to our observed bands. A further aspect that should receive consideration is the fact that in Raman measurements above T_c a new mode at 826 cm^{-1} is observed [25]. This upcoming new mode at 826 cm^{-1} clearly does not appear in our measured FTIR spectra. We can therefore assign this mode as a nearly ideal v_1 stretching mode in SeO_4 tetrahedra, that is not IR active. At the same time, we are also observing lower symmetric $v_1[SeO_4]^{2-}$ modes (812 cm^{-1} at 503 K), which are associated with $v_1[HSeO_4]^{1-}$ modes (833 cm^{-1} at 503 K). So the observed modes can be classified in two groups differing by the strength of the $[SeO_4]^{2-}$–$[HSeO_4]^{1-}$ coupling degree (Table 9). Both groups result from non-centrosymmetric

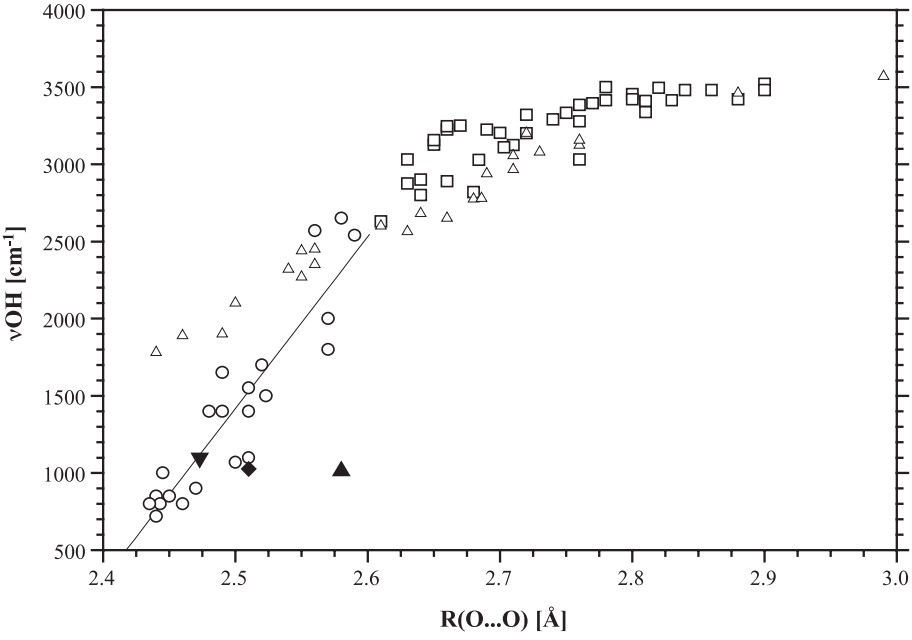

Fig. 10. Frequency of the OH stretching mode νOH as a function of the O(2)–O(2)′ distance [$R_{(O\ldots O)}$]; open symbols: comparison with literature data (circles: Ref. [24], 2.4 to 2.6 Å with linear fit (solid line); squares: Ref. [24], 2.6 to 3.0 Å; upward triangles: Ref. [25]); solid downward triangle: our TFXA measurement at 60 K, with literature distance $R_{O(2)–O(2)'}$=2.47 Å [3]; solid diamond: our IR single crystal spectra at 298 K, with literature distance $R_{O(2)–O(2)'}$=2.51 Å [26]; solid diamond: IR single crystal spectra at 298 K with literature distance $R_{O(2)–O(2)'}$=2.51 Å [26]; solid upward triangle: IR single crystal spectra at 503 K with literature distance $R_{O(2)–O(2)'}$=2.58 Å [26].

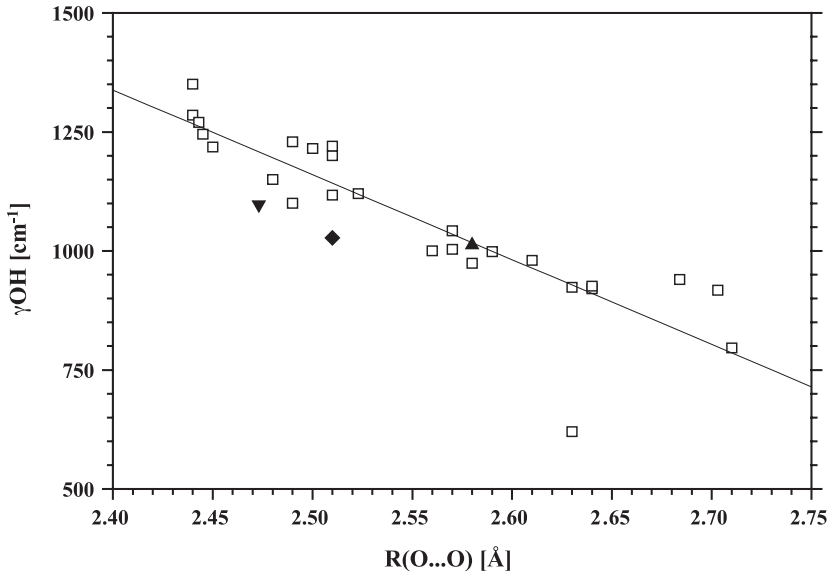

Fig. 11. Frequency of the OH bending mode γOH (out-of-plane) as a function of the O(2)–O(2)′ distance [$R_{(O\ldots O)}$]; open square: comparison with literature data [24]; solid downward triangle: TFXA measurement at 60 K with literature distance $R_{O(2)-O(2)'}$=2.47 Å [3]; solid diamond: IR single crystal spectra at 298 K with literature distance $R_{O(2)-O(2)'}$=2.51 Å [26]; solid upward triangle: IR single crystal spectra at 503 K with literature distance $R_{O(2)-O(2)'}$=2.58 Å [26].

$H[SeO_4]_2^{3-}$ dimers. The intensities of the weakly coupled monomers increase, those of strongly coupled monomers decrease upon making the transition to the high-temperature phase. The intensity changes are observable in a fairly broad temperature range, below and above the phase transition (T_c=449 K).

5. Discussion of the results and conclusion

On the basis of the centrosymmetric space group symmetries, a decrease of the number of vibrational modes upon crossing the phase transition region towards the high-temperature phase would have to be clearly observable, in the examined frequency and temperature range, however, this is not the case. The assumption of (transient) local non-centrosymmetric space group symmetries solves this problem. This has led us to propose the local short-time presence of such lower symmetries in the context of and as a characteristic feature of the mechanism of proton conduction and diffusion.

A certain number of vibrational modes exhibit strong temperature dependences of their amplitudes, which are apparently related with the appearance of protonic conductivity in the neighbourhood of the SSPC phase transition (449 K). This observation suggests a strong increase of the concentration of the $[HSeO_4]^{1-}$ monomer upon crossing the phase transition temperature. The present results from FTIR and from IINS measurements (using TFXA and NEAT) indicate that an essential ingredient of the mechanism of proton conduction in $Rb_3H(SeO_4)_2$ is the H-bond formation/H-bond breaking equilibrium reaction required for the exchange of protons occurring within the H-bond and between neighbouring hydrogen bridges (Fig. 12). This leads to temperature dependent “concentrations” of selenate monomers and dimers, with high dimer concentration at low temperatures and high monomer concentrations at the high temperatures of the SSPC phase.

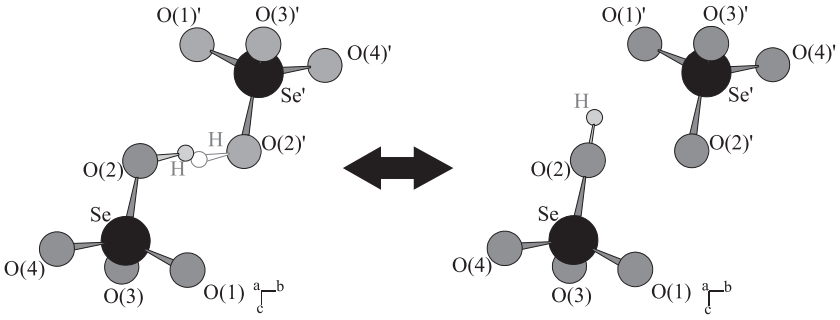

Fig. 12. Schematic picture of the H-bond formation/H-bond breaking reaction equilibrium in $Rb_3H(SeO_4)_2$. The $H[SeO_4]_2^{3-}$ dimer breaks into $[SeO_4]^{2-}$ and $[HSeO_4]^{1-}$ monomers which reunite subsequently to form again a dimer. (Note that the partner in this formation is not necessarily the same as before, but may be a different neighbour.)

Acknowledgements

This investigation was supported by the Deutsche Forschungsgemeinschaft (Project No. LA 324/33-1 and 2). We are indebted to the Rutherford Appleton Laboratory, Chilton, for providing the TFXA instrument for our IINS measurements, to Dr. S.F. Parker for some technical assistance with the measurements and to Dr. J. Tomkinson for useful discussions.

References

[1] A.I. Baranov, I.P. Makarova, L.A. Muradyan, A.V. Tregubchenko, L.A. Shuvalov, V.I. Simonov, Sov. Phys. Crystallogr. 32 (1987, 1988 AIP) 400–407.
[2] A. Pawlowski, L. Szczesniak, M. Polomska, B. Hilczer, L. Kirpichnikova, Solid State Ionics 157 (2003) 203–208.
[3] R. Melzer, R. Sonntag, K.S. Knight, Acta Crystallogr., C Cryst. Struct. Commun. 52 (1996) 1061–1063.
[4] R. Melzer, T. Wessels, M. Reehuis, Solid State Ionics 92 (1996) 119–127.
[5] T. Gustafsson, M. Ichikawa, I. Olovsson, Solid State Commun. 115 (2000) 473–476.
[6] Yu.I. Yuzyuk, V.P. Dmitriev, L.M. Rabkin, I. Gregora, F. Smutny, L.A. Shuvalov, Solid State Ionics 91 (1996) 145–153.
[7] R.E. Lechner, G. Schuck, K. Langer, J. Phys. Soc. Jpn. 70 (2001) 274–276.
[8] G. Schuck, R.E. Lechner, K. Langer, Appl. Phys. 74A (2002) 1098–1100.
[9] R.E. Lechner, Solid State Ionics 61 (1993) 3–11.
[10] R.E. Lechner, Ferroelectrics 167 (1995) 83–98.
[11] T. Springer, R.E. Lechner, Diffusion studies of solids by quasielastic neutron scattering, in: P. Heitjans, J. Kärger (Eds.), Diffusion in Condensed Matter—Methods, Materials, Models, Springer-Verlag, Berlin, 2005, pp. 87–161, Chap. 3, in press.
[12] R.E. Lechner, Solid State Ionics 145 (2001) 167–177.
[13] G. Schuck, R.E. Lechner, in press.
[14] G. Schuck, PhD thesis, Technische Universität Berlin (2000).
[15] K. Nakamoto, Infrared Spectra of Inorganic and Coordination Compounds, Wiley-Interscience, New York, 1970.
[16] V. Železný, J. Petzelt, Yu.G. Goncharov, G.V. Kozlov, A.A. Volkov, Solid State Ionics 89 (1989) 175–178.
[17] G. Suresh, R. Ratheesh, V.U. Nayar, M. Ichikawa, G. Keresztury, Spectrochim. Acta 51A (1995) 429–435.
[18] W.G. Fateley, F.R. Dollish, N.T. McDevitt, F.F. Bentley, Infrared and Raman Selection Rules for Molecular and Lattice Vibrations—The Correlation Method, Wiley-Interscience, New York, 1972.
[19] V. Železný, J. Petzelt, A. Pawlowski, A.I. Baranov, N.M. Shchagina, Ferroelectrics 107 (1990) 145–149.
[20] G. Suresh, R. Ratheesh, V.U. Nayar, M. Ichikawa, Spectrochim. Acta 52A (1996) 465–470.
[21] Y. Matsumoto, J. Phys. Soc. Jpn. 67 (1998) 2215–2217.
[22] G.E. Walrafen, J. Chem. Phys. 39 (1963) 1479–1492.
[23] R. Paetzold, H. Amoulong, Z. Anorg. Allg. Chem. 317 (1962) 166–167.
[24] A. Novak, Structure and Bonding, vol. 18, Springer Verlag, Berlin, 1974, pp. 177–216.
[25] K. Nakamoto, M. Margoshes, R.E. Rundle, J. Am. Chem. Soc. 77 (1955) 6480–6486.
[26] A. Bohn, Diploma thesis, Technische Universität Berlin (1994).
[27] R.E. Lechner, R. Melzer, J. Fitter, Physica. B 226 (1996) 86–91.
[28] B. Rufflé, J. Ollivier, S. Longeville, R.E. Lechner, Nucl. Instrum. Methods A 449 (2000) 322–330.
[29] S.F. Parker, K.E. Horton, J. Tomkinson, The TFXA User-Guide. Internal Report No. RAL-95-036, Rutherford Appleton Laboratory, Chilton, UK (1995).
[30] A.V. Belushkin, J. Tomkinson, L.A. Shuvalov, J. Phys., France 3 (1993) 217–225.
[31] G.J. Kearley, Nucl. Instrum. Methods Phys. Res., Sect. A, Accel. Spectrom. Detect. Assoc. Equip. 354 (1995) 53–58.